Energy-tunable transmission x-ray microscope for differential contrast imaging with near 60 nm resolution tomography

Gung-Chian Yin
National Synchrotron Radiation Research Center, 101 Hsin-Ann Road, Hsinchu 30076, Taiwan and Department of Photonics and Display Institute National Chiao Tung University, Hsinchu 300, Taiwan

Mau-Tsu Tang, Yen-Fang Song, Fu-Rong Chen, and Keng S. Liang
National Synchrotron Radiation Research Center, 101 Hsin-Ann Road, Hsinchu 30076, Taiwan

Frederick W. Duewer and Wenbing Yun
Xradia Inc., 5052 Commericial Circle, Concord, California 94520

Chen-Hao Ko
Department of Electrical Engineering, Yuan Ze University, 135 Yuan Tung Road, Chungli 320, Taiwan

Han-Ping D. Shieh
Department of Photonics and Display Institute, National Chiao Tung University, Hsinchu 300, Taiwan

(Received 30 December 2005; accepted 14 May 2006; published online 15 June 2006)

An energy-tunable transmission hard x-ray microscope with close to 60 nm spatial resolution in three dimensions (3D) has been developed. With a cone beam illumination, a zone plate of 50 nm outmost zone width, a stable mechanical design, and software feedback, we obtained tomographic data sets that are close to 60 nm spatial resolution. Meanwhile, the element specific imaging was also obtained by a differential absorption contrast technique used below and above the absorption of the element. Examples of advanced intergraded circuit devices are used to demonstrate the element selectivity and spatial resolution in 3D of the microscope. © *2006 American Institute of Physics*. [DOI: 10.1063/1.2211300]

The development of a high resolution transmission x-ray microscope[1–3] (TXM) has been actively pursued since the availability of synchrotron sources. In the soft x-ray region (100 eV–1 keV), a zone plate[4–7] based TXM has achieved a spatial resolution of 15 nm.[8] However, such a resolution has been a big challenge in the hard x-ray region due to the difficulty of zone plate fabrication. In the hard x-ray region, tomographic resolution approaching 400 nm by a compound reflective lens has been reported.[9]

In this letter, we report the construction of such a microscope at the National Synchrotron Radiation Research Center (NSRRC), which can operate in the photon energy range between 8 and 11 keV with better than 60 nm spatial resolution[10] in two dimensions (2D), and tomographic images at close to 60 nm voxel resolution. With energy from 8 to 11 keV, silicon-based samples with a thickness of 100 μm can be imaged nondestructively. Elements with absorption edges between this photon energy range can be detected using the technique of differential absorption contrast imaging.

The microscope is installed at Beamline BL01B (Ref. 11) of NSRRC with a superconducting wavelength shifter (SWLS) source, which provides a measured photon flux of 4.5×10^{11} photons/s/0.1%bw in the energy range 5–20 keV. The x-ray beam is focused by a toroidal shaped focusing mirror (FM) with a focal ratio nearly equal to 1:1. A double crystal monochromator (DCM) using a pair of Ge(111) crystals tunes the x-ray energy in the 8–11 keV range, with an energy resolving power of better than 1000 that matches the zone number of the objective zone plate; in the present case it is ~400. The energy range 8–11 keV is thus chosen in order to cover the absorption edges of Cu, Zn, Ga, Ge, As, Ta, W, Au, Hg, Pb, etc., the most important elements for semiconductor industries. After the focusing mirror and Ge(111) DCM, the x rays are further shaped by a capillary condenser.[12,13] The condenser is a circularly symmetric single reflection glass capillary optic whose profile is custom made according to the characteristic of the incident beam. Its entrance aperture is about 300 μm and with an end opening about 200 μm and 15 cm length. This capillary condenser gives the reflection angle of 0.5 mrad with respect to the propagation direction. The measured reflection angle from the condenser is from 0.87 to 1.13 mrad. A gold bead is attached to the end of the condenser so that a hollow cone beam of illumination is generated. The beam is then focused on the sample position. After traveling a distance of the focus length of zone plate, 27 mm in this case, the zone plate of 70–85 μm diam is well illuminated by the cone beam generated by the capillary condenser.

Due to the emittance of the synchrotron source in the horizontal and vertical directions, which are quite different, there is a tradeoff between brightness and uniformity of the image. The synchrotron source is always in elliptical in shape and has a wide spread in a horizontal direction. Because of the difference between the horizontal and vertical emittances is about several orders of magnitude, it is hard to balance the illumination of the vertical and horizontal directions. The way we use to match the source is to adjust only the beam line so that the positions of the vertical and horizontal focis are at the same position after the condenser for optimizing the flux.

For a Fresnel zone plate, the diffraction-limited resolution is $1.22dr$, where dr is the outermost zone width. The zone plate is made by electroplating gold on the silicon nitride membrane; the thickness of gold is 890 nm, which gives a retardation of about $\pi/2$, and the test efficiency of

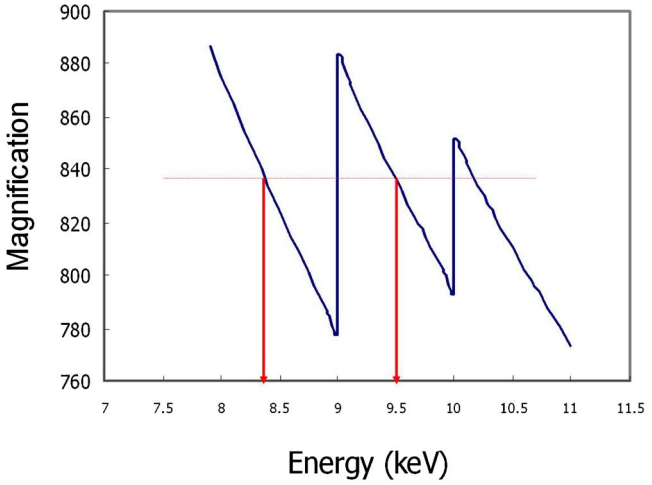

FIG. 1. The calculated magnification vs energy from 8 to 11 keV. The magnification varies between 780 and 110 for the 8–11 kev x-ray energy range due to the focal length of zone plate changes with the x-ray energy. To minimize variation of the image magnification and focal length variation, three zone plates with different diameters are used. Furthermore, it is desirable to choose the same magnification for different energy to do the image subtraction under and above the absorption edge.

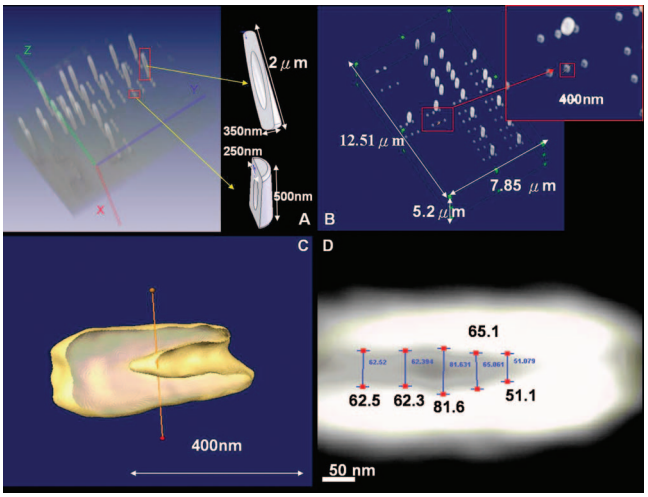

FIG. 2. (a) (Color) 3D rendering of tungsten plug with a keyhole and the diagrams showing the structure of the keyhole (right to) and the tungsten plug with a 350 nm diam. (Right bottom) The tungsten plug with a 250 nm diameter. (b) The 3D rendering of the tungsten plug is plotted with higher threshold. The wire made of a copper-aluminum alloy is removed from the rendering; the tungsten distribution is shown. The red region of the left picture is the region of the right picture. The red region in the right picture is the tungsten plug, which is analyzed in (c). (c) The top view and side view of the tungsten plug displayed in a voxel mode (top) and an isosurface (bottom) mode. The orange line indicates the region of the cross-section plot that is shown in Fig. 3. (d) The measurement of the size of the keyhole. The diameters of the keyhole range from 50 to 80 nm.

first order diffraction is above 10%. Using a zone plate with a 50 nm outermost zone width, we are able to achieve 60 nm diffraction-limited spatial resolution with well engineered mechanical and thermal stability. By acquiring a series of 2D images with the sample rotated stepwise, three-dimensional (3D) tomographic data can be reconstructed and rendered.

The software is developed to calculate the center of rotation of the sample from each angle and then the computer can automatically perform tomographic data acquisition. Due to the vibration and the wobble of the rotation stage, the misalignment in the horizontal and vertical directions could be several micrometers, which requires the automatic alignment process in the software. The alignment of data is processed by a phase correlation method,[14,15] which is a modified method from the cross correlation[16] method and it sharpens the correlation function of the two images. The tomography data set can be automatically aligned and reconstructed by the software.

The focal length of a zone plate lens is proportional to x-ray energy. To cover the 8–11 keV operational x-ray energy for the x-ray microscope in which the detector is kept stationary for stability, three zone plates are used to minimize any change of the magnification of x-ray imaging as a function of x-ray energy. The diameters of the three zone plates are 85, 75, and 70 μm, respectively. With these diameters, the three zone plates have approximately the same focal length for 8.5, 9.5, and 10.5 keV x rays, respectively.

The total image magnification is equal to the product of x-ray image magnification and the optical magnification of 20. The total image magnification is from 780–880 in 8–11 keV, corresponding to an about 12% variation, as shown in Fig. 1. With the design, the sample can be imaged by different energies with the same image magnification if the two energies are chosen precisely.

We show an interesting application of the TXM in imaging the defective tungsten plugs, which interconnect the different layers of the integrated circuit (IC). The issue often encountered in the tungsten plug is a defect in its center, which is called a "keyhole" formed in the electroplating process of tungsten. The keyhole can cause the breakdown of the circuit. For x-ray microscopy measurements at 8–11 keV, the preferable thickness of silicon-based IC is below 50 μm, which gives the transmission from 50% to 70% at normal incidence, and gives 12%–42% at an angle of 70°.[17] The general preparation process of silicon-based IC is thinning at the back of the silicon side down to a thickness of about 150 μm and then dimples[18] the silicon side further down to 50 μm.

The tomography datasets are also reconstructed from 141 images, from −70° to +70°, which is taken under 10.5 keV, above the absorption edge of the tungsten (10.1 eV). The exposure time for a 0° image is 1 min, and it increases according to the angle between the sample normal and input beam.

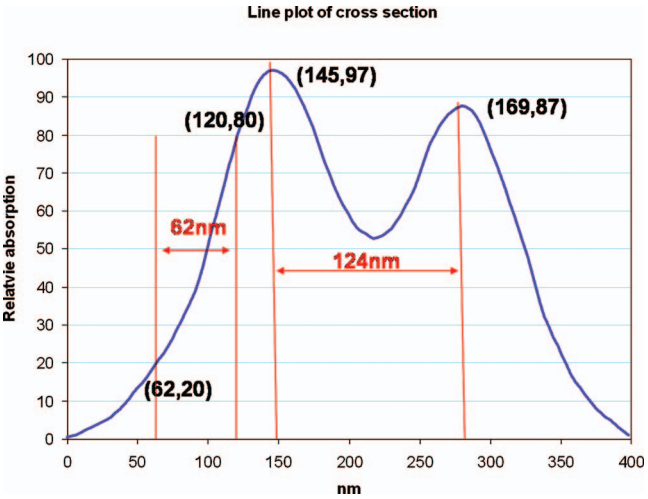

FIG. 3. (Color) The cross-section plot of the orange line in Fig. 2. The resolution is estimated and is near 60 nm.

The reconstructed image shown in Fig. 2(a) and the cross-section diagram indicates the tungsten plugs of 350 and 250 nm with a keyhole whose diameter is measured in Fig. 2(d). Figure 2(b) shows the 3D rendering image from which the low absorption of alloy of copper and aluminum is removed. Therefore, the Fig. 2(b) shows a clear tungsten distribution. The tomography data sets consist of an area of 12.51 μm $\times$ 7.85 μm $\times$ 5.2 μm. A closer image is shown in the right part of Fig. 2(b), where the red boxed region indicates the area to be analyzed. The region is a 250 nm tungsten plug with a keyhole inside. The original data in this area were cropped and interpolated for smoothing the data. The interpolated data are shown in Fig. 2(c), which is the side-view displayed by the isosurface mode showing the size of the hole three dimensionally. The line plot of the orange line in Fig. 2(c) is shown in Fig. 3. The vertical axis is the relative absorption, which is converted from the original tomography dataset. The maximum absorption is set to 100, and the minimum absorption is set to 0. The horizontal axis is the distance, which is 400 nm in the line plot. The plot shows the cross section of the keyhole, therefore, there are two local maximums of the absorption indicating the walls of the tungsten plug. The first maximum and second maximum is at 60 and 210 nm, respectively. The resolution of the tomography dataset can be judged as the absorption goes from 20% to 80% (Ref. 19) in 62 nm, and the period is in 124 nm. We conclude that the half-pitch period of tomography is around 60 nm. The diameter of this keyhole is estimated from 50 to 80 nm as shown in Fig. 2(d). On average, the size of a keyhole is about 75 nm.

In summary, we have demonstrated the methodology of implementing a tunable transmission microscope for synchrotron source and the tomography data calculated from a limited angle (+70° to −70°) datasets that are close to 60 nm tomographic spatial resolution. Meanwhile, using the contrast above the x-ray absorption edge, the image element specific is also demonstrated by investigating the keyhole of the tungsten plug.

The authors thank Sara Tsai from Powerchip Semiconductor Inc. (PSC) for providing the tungsten plug sample, Te-Hui Lee for the beamline control program setup, and the staff of the Beamline Division of NSRRC for their support in this project.

[1]Gerd Schneider, Ultramicroscopy **75**, 85 (1998).
[2]U. Neuhäusler, G. Schneider, W. Ludwig, and D. Hambach, J. Phys. D **36**, 79 (2003).
[3]W. Meyer-Ilse, H. Medecki, J. T. Brown, J. Heck, E. Anderson, C. Magowan, A. Stead, T. Ford, R. Balhorn, C. Petersen, and D. T. Attwood, *X-ray Microscopy and Spectromicroscopy* (Springer, Berlin, 1997).
[4]E. Di Fabrizio, F. Romanato, M. Gentili, S Cabrini, B. Kaulich, J. Susini, and R. Barrett, Nature (London) **401**, 895 (1999).
[5]B. Lai, W. B. Yun, D. Legnini, Y. Xiao, J. Chrzas, and P. J. Vidcaro, Appl. Phys. Lett. **61**, 1877 (1992).
[6]W. Yun and B. Lai, Rev. Sci. Instrum. **70**, 3537 (1999).
[7]W. Yun, B. Lai, Z. Cai, J. Maser, D. Legnini, and E. Gluskin, Rev. Sci. Instrum. **70**, 2238 (1999).
[8]W. Chao, B. D. Harteneck, J. A. Liddle, E. H. Anderson, and D. T. Attwood, Nature (London) **435**, 1210 (2005).
[9]C. G. Schroer, J. Meyer, M. Kuhlmann, B. Benner, T. F. Günzler, B. Lengeler, C. Rau, T. Weitkamp, A. Snigirev, and I. Snigireva, Appl. Phys. Lett. **81**, 1527 (2002).
[10]G.-C. Yin, F. Duewer, Y.-F. Song, M.-T. Tang, W. Yun, and K. S. Liang, IPAP Conference Series 7, Proceedings of the 8th International Conference on X-Ray Microscopy (XRM2005), Himeji, 2005, p. 258.
[11]Y. F. Song, C. H. Chang, C. Y. Liu, L. J. Huang, S. H. Chang, J. M. Chuang, S. C. Chung, P. C. Tseng, J. F. Lee, K. L. Tsang, and K. S. Liang, AIP Conf. Proc. **705**, 412 (2004).
[12]B. Murphy, D. L. White, Alastair A. MacDowell, and Obert R. Wood, Appl. Opt. **32**, 6920 (1993).
[13]D. H. Bilderback, D. J. Thiel, R. Pahl, and K. E. Brister, J. Synchrotron Radiat. **1**, 37 (1994).
[14]R. C. Gonzalezand and R. E. Woods, *Digital Image Processing* (Addison-Wesley, New York, 1992), p. 109.
[15]J. S. Tsai, J. J. Kai, L. Chang, and F.-R. Chen, J. Electron. Microsc. **53**, 1 (2004).
[16]C. D. Kuglin and D. C. Hines, *Proceedings of IEEE International Conference on Cybernetics and Society* (IEEE, New York, 1975), pp. 163–165.
[17]http://www-cxro.lib.gov, Center of X-ray Optics.
[18]http://www.gatan.com/specimenprep/
[19]B. Lengeler, C. G. Schroer, M. Richwin, J. Tümmler, M. Drakopoulos, A. Snigirev, and I. Snigireva, Appl. Phys. Lett. **74**, 3924 (1999).